Chapter 2
MEMS Microhotplate Constraints

Ferenc Bíró, Zoltán Hajnal, István Bársony and Csaba Dücső

2.1. State of the Art

2.1.1. Micro-heaters and Their Applications

Microhotplates provide elevated temperatures up to 800-1000 °C by resistive Joule heating of the integrated filament to enable chemical reactions on the heated surface or facilitate physical changes in their vicinity. Devices utilizing microhotplate structures for local heating are classified in Fig. 2.1 according to the operation temperature. In principle, when operation below 450-500 °C is needed, e.g. in bio-platforms, semiconductive metal oxide (MOX) chemical sensors, flow sensors and actuators the high temperature related degradation phenomena don't have to be considered. The microhotplate itself is thereby not a limiting factor in the long-term, stable operation of those devices.

The operation temperature of the thermo-catalytic gas sensors is determined by both the target gas and the applied catalyst. Therefore, the presented hydrogen sensors operate around 150-250 °C, whereas most of the methane sensors require much higher temperatures up to 700-800 °C.

Microhotplates are also used in thermal conductivity type sensors [1]. As the thermal conductivity of gases (especially methane) increases with temperature, the higher the temperature the higher is also the sensitivity of the device. When known gas composition is investigated, thermal conductivity can be utilized in gas flow (mass flow) and pressure (Pirani) measurements as well [2, 3].

Moreover, the sensitivity of the above devices can also be increased by application of high TCR material for filament or for the integrated thermometer. In discrete devices operating up to a few hundred °C, the chemically stable Pt is commonly used [4-13]. Although polycrystalline silicon is the obvious choice in a CMOS integrated smart device [13-16] the maximum temperature applicable is inherently limited by the MOS circuit. For high

Csaba Dücső
Centre for Energy Research, Budapest, Hungary

temperature operation the most attractive material is single crystalline silicon [17-19]. Micro-heaters were formed from the device layer of a SOI wafer and tested in thermal conductivity methane sensors at temperatures up to 900 °C [19].

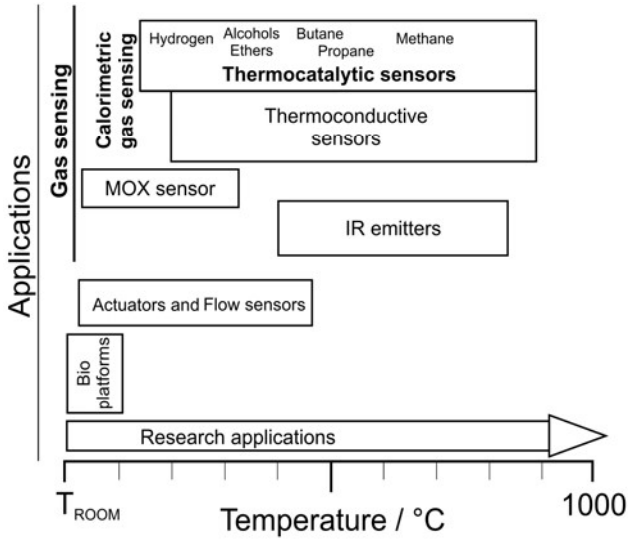

Fig. 2.1. Classification of devices making use of high temperature by locally heated microhotplates.

The most intensively investigated gas sensors so far operate by chemisorption driven conductivity change of semiconductive metal-oxide layers, often called MOX. Apart from a few exemptions MOX sensors operate in the range of 100-400 °C. They are thus less sensitive for moderate temperature fluctuations; thereby no specific requirements are associated with the heater of the hotplate [20].

Moderate temperatures up to a few tens or maximum two hundred °C are required in some thermomechanical actuators presented in [21], like in thermal expansion of paraffin actuators heated by aluminium filament [22, 23].

IR emitters applying microfilaments may become novel elements in non-dispersive IR gas sensors. To enhance the sensitivity of these devices, indirect wavelength selective thermal emitters had been fabricated from metal filaments to generate IR radiation [24]. These filaments have to operate in the mid-infrared up to 1000 K or even above in the near-infrared region [25].

2.1.2. Essential Requirements

Although the essential requirement of microhotplate performance is uniformity, the emphasis is also put on different properties when selecting the “best” structure for a particular commercial or research application.

Most important in a commercial device is the stability during the minimum year–long lifetime next to the low power dissipation and reproducible operation as well as the low production costs, whereas the knowledge of the real temperature and temperature distribution across the hotplate surface is rather marginal as long as it does not jeopardize the functionality.

The exact temperature profile and its stability are, however, essential for research purposes, especially when catalytic chemical processes are exploited during operation. The long-term stability, power consumption and lifetime issues are not critical, as long as they are adequate for to the period of investigation.

The knowledge of exact temperature across the microhotplate is crucial when studying catalytic reactions of nanomaterials (as called as nanoreactors) [26]. Most important is the accuracy and stability in settling and read-out of temperature, however exact knowledge of ambient composition and pressure is also required. These strict operation conditions of catalytic devices together with the expected lifetime can be essential in industrial environment as well.

In biochemical research, like in platforms for food kinetics [27], the constant temperature uniformity and extremely accurate setting up to 100 °C is targeted.

2.1.3. Mechanical Design and Structural Materials

Microhotplates can be classified according to their geometry, quality of structural materials applied in the heater and in the membrane. The temperature read-out can be provided by an additional temperature sensor or by the change of resistance of the filament itself.

In terms of geometry fundamentally full- or perforated-membrane solutions can be distinguished. While the full-membrane versions offer better mechanical stability, the suspended hotplates exhibit 5-10 % more efficient thermal isolation at atmospheric pressure, meaning proportionally less power dissipation [8, 28-30]. The heater is typically suspended by 1, 2 or 4 arms upon the variety of filament geometry [50-52]. Alternative structures for peripheral- and full-surface heating are proposed using various layouts, such as simple Ω-shape [9], rectangular meander, double meander, double spiral meander and some exotic geometry as well [10, 14, 17].

Apart from the few MOS-channel heating solutions, in most of the devices Pt or polycrystalline silicon forms the filament, but for IR emitters and gas sensors Cr, W, SiC and TiN were also proposed [24, 31, 32, 52]. Note that the use of poly-crystalline silicon is limited to the low or medium temperature range due to re-crystallization at higher temperatures [14]. By introduction of SOI wafers single crystalline silicon emerged as a promising filament material candidate [17, 48]. Beside thermomechanical stability of the membrane (cracking) the filament geometry and the quality of filament material are considered as the most important factors in device degradation [33]. According to the generally accepted rule the maximum obtainable filament temperature to maintain integrity goes up to 30 % of its melting point (Hüttig temperature). Nevertheless, the real

picture is more complex; phase transitions, recrystallization and chemical reactions must also be considered as seen from data in Table 2.1.

Tungsten should stand extreme high temperature, however its chemical reactivity limits the application in vacuum or specific environment (see incandescent lamps). Concerning activation energies of degradation, poly-crystalline silicon should exhibit better stability than Pt, but due to re-crystallization and interface phenomena involved its superiority is questionable.

Table 2.1. Material properties and activation energies of degradation of some filament materials [13, 34].

Material	Melting point (°C)	Hüttig temperature (°C)	Activation energy of degradation (eV)
Pt	1768	530	2,2
W	3422	1026	–
Si	1411	423	4,2

The stress induced thermo-mechanical failures described in [35, 36] led to the application of various materials and multilayer structures for the isolated membrane. The common feature of the proposed structures is to provide the best thermo-mechanical properties and to maintain device stability and integrity during operation. Concerning the structural materials, SiO_2, Si_3N_4, SiO_xN_y, Si-rich SiN_x and their multilayered combinations dominate. Besides, SiC, porous silicon and porous alumina have also been reported [7, 16]. For residual stress values below 100 MPa stress compensated multilayer structures were proposed by Laconte and Rossi [36, 37].

Independent temperature reading is optional and rarely applied. It is typically used in peripheral heating solutions [9, 11, 29], or when the TCR of the filament material is too low to allow accurate measurements of the temperature dependent resistance changes. Due to the low applied current in the additional embedded resistor the chance of electromigration related degradation can be disregarded [38, 39].

Apart from the still marginal IR emitter function micro-heaters used in catalytic-calorimetric devices are exposed to the most extreme conditions. High temperatures are used in various gaseous environments, especially when the targeted gas is e.g. methane. The operation temperature is determined by the catalyst activity; i.e. in case of *thermocatalytic* sensors for Pd-Pt and Pt catalysts the operation temperature should exceed 450 °C [12, 40] and 600 °C [9], respectively.

Due to those high operation temperatures severe reliability problems arise in the hotplate structure. Phase changes, inter-diffusion, migration phenomena and chemical reactions (oxidation, corrosion) can lead to filament layer adhesion problems and fatal mechanical or structural damages [53-56]. As the relationship between temperature and deterioration rate follows an exponential-like function, the higher the required operation temperature the more challenging is the fabrication of a reliable hotplate. Consequently, to find the

best design and construction materials, the potential degradation mechanisms must be identified first. Therefore, in this chapter we focus on the identification and characterization of the major degradation mechanisms of microfilaments used in *thermocatalytic* gas sensors above 500 °C.

2.2. Structure and Reliability

2.2.1. Effect of Temperature Gradients

In our previous work we established a correlation between the position of thermal gradients and defect sites both in meander- and double spiral type Pt filaments [41]. If the temperature gradient exceeds 0.4 K/μm and the temperature is over 1000 K the cumulative effect of thermally driven thermo-migration and electron flow driven induced electromigration result in filament ruptures at well-defined locations of the filament. There the thermal gradient of the non-uniform temperature distribution along the filament is the highest and the direction of the cumulative mass transport originating from both above phenomena coincide (Fig. 2.2).

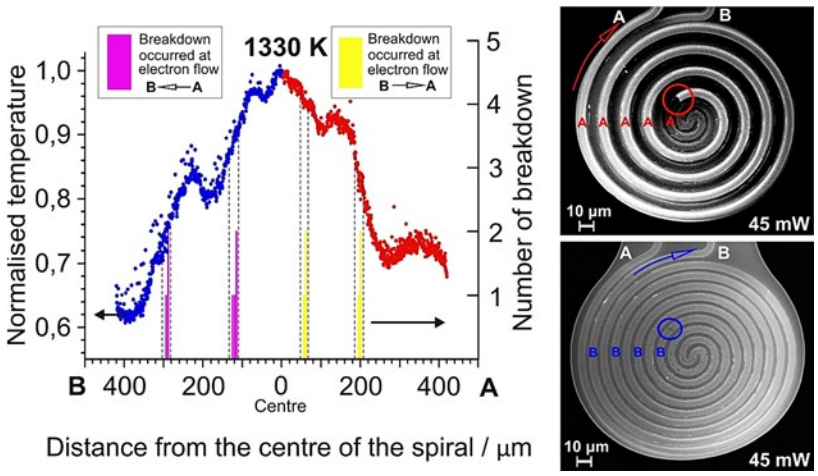

Fig. 2.2. Positions of ruptures along the rolled-out filament of identical double spiral microhotplates. Twice eight different hotplates were investigated powering each by 45 mW, but applying opposite current directions for each as indicated in the SEM images. The positions of the ruptures clearly reveal the decisive importance of the thermal gradient and the coincidence of the two identified mass transport phenomena.

2.2.2. Microhotplate Designs Investigated

Realizing the crucial role of temperature non-uniformity and the accompanying high gradient in device failures alternative designs of micro-heaters were fabricated and tested (Fig. 2.3). The aim targeted by the new layouts is threefold:

- Obtaining uniform temperature on a larger area, thereby eliminating the extreme high temperatures in the center of the hotplates;
- Reduction of critical; temperature gradients along the filament, especially where the temperature is over c.a. 500 °C;
- Testing the single-crystal silicon heater for durability at high temperature operation.

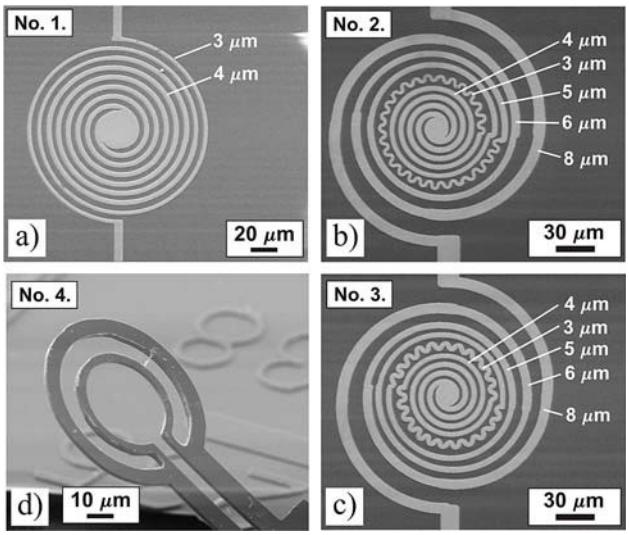

Fig. 2.3. New layout designs of filaments. Double spiral Pt meanders of modified geometries aim at improved temperature uniformity (a, b, c) and tailored temperature gradient (b, c). Single-crystalline silicon heater for durability tests (d).

Pt filaments of modified double spiral geometries were designed for achieving better temperature uniformity with less temperature gradient. Hotplates No. 1, No. 2 and No. 3 in Fig. 2.3 have an increased size Pt plate in the center to homogenize the temperature. By narrowing the filament in all the 3 layouts around the central region we also target the expansion of the uniform area. Moreover, in structures No. 2 and No. 3 the elongated and step by step widened interconnections at the perimeter serve to attenuate the temperature gradient.

All structures are full-membrane type and have the same filament composition with 25/300/25 nm TiO_x/Pt/TiO_x thickness as used in our previous works [41].

Single-crystal silicon cantilever type microheaters were fabricated from the 2 μm thick n-doped device layer of an SOI wafer (Fig. 2.3, No. 4). The filament is coated with 100 nm SiO_2 layer to passivate the surface at high temperature operation (700-800 °C).

The test conditions applied are summarized in Table 2.2. The conditions of reference cantilever suspended duble spiral type heater can be found in [42].

Table 2.2. Filament properties and lifetime test conditions for microheaters.

Device number	No. 1.			No. 2.	No. 3.	No. 4.
Filament material	Pt			Pt	Pt	Monocrystalline Si
Heating power (mW)	35	40	45	40	40	28

2.3. Reliability Issues

2.3.1. Importance of Capping Layer

As the hotplates are operated in various gas compositions at atmospheric conditions, the filament material must be protected regardless of its quality. Direct exposure to air at the high test-temperatures leads to fast degradation by rapid oxidation. Therefore, micro-heaters in this study were completely covered with SiO_2 diffusion barrier layers (capping layer).

In order to prove the detrimental effect of filament oxidationthe lifetime of identical cantilever type micro-heaters were parallel tested. At the perimeter of four hotplates the SiO_2 capping layer was removed, leaving the edge of the outer Pt ring exposed to the ambient. Devices together with their intact references were driven by 37 mW until breakdown. The lifetime of the bare devices was 2-3 hours, whereas the references run for 81 hours [42].

SEM investigations revealed that all the failures were located at the perimeter of the device, where the capping layer was removed and the Pt filament was directly exposed to air (Fig. 2.4).

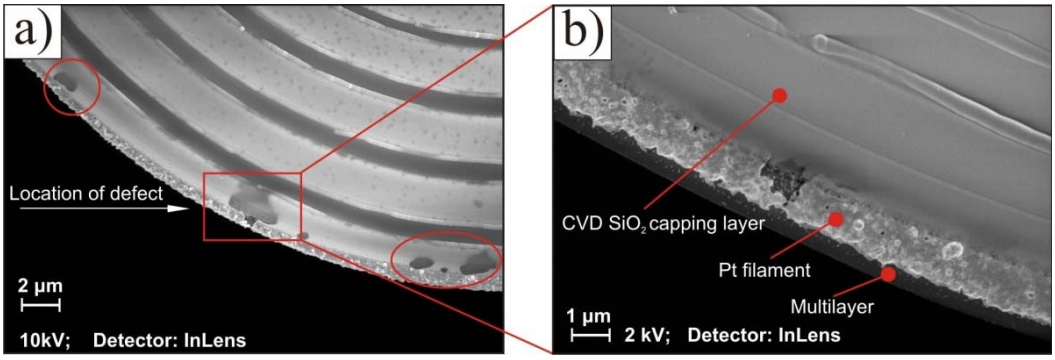

Fig. 2.4. (a) SEM images of an incompletely covered Pt filament taken after breakdown. The capping layer was removed from the edge of the outer ring. Several defect sites can be identified as indicated. All of them start to growth from the non-covered edge and protrude inside. (b) Closer view.

In Fig. 2.4a six deffect sites can be recognised, all at the edge of the non-covered ring of filament. The exact mechanism of this phenomenon is unknown but the lifetime measurements clearly show the necessity of protective covering. The appearance of the defect site looks like a cavity formed underneath the capping layer, similar to defect sites caused by Pt mass transport at the higher teperature regions of the filament. Note, that in case of the uncovered Pt filament the process is much faster, although the temperature at the perimeter is the lowest.

2.3.2. Lifetime and Activation Energies

Resistance-time curves are used to characterize the stability of microheaters, to distinguish different phenomena and to deduce the activation energies of the different stages of degradation.

In Fig. 2.5 resistance-time curves of cantilever suspended, double spiral Pt filaments are illustrated. The "S" shape of the curves is the consequence of the complex degradation mechanisms, i.e. phase changes in the adhesion layer and the thermo- and electro-migration mass transports as reported earlier [42]. Furthermore, all the curves have to be divided into two sections by the inflection points (indicated by black circles in the figure). These points were identified by the location of minima of the first time-derivate. The change of resistance in the vicinity of inflection can be explained by two activation energies (E_{a1} and E_{a2}). These were calculated from the Arrhenius plots in Fig. 2.5b, constructed from the rate of resistance changes measured at four average surface temperatures. The activation energies E_{a1} and E_{a2} are 1.7 eV and 2.1 eV, respectively. Considering the position of the inflection points in each individual curve we may state that the time elapsed until the inflection point decreases at higher temperatures but time elapsed after the inflexion point until the breakdown decreases by smaller amounts. This observation fits to the expectation based on the magnitude of the activation energies. The first activation energy region can be associated with the formation and intrusions of growing TiO_2 grains in the Pt filament [42].

In terms of lifetime and device stability this is crucial, because this effect gradually reduces the lifetime of the filament and manifests itself in a continuous drift of device parameters. The value of the second activation energy (E_{a2} = 2.2 eV) characterizes the migration of Pt along those sections of the filament, where the directions of the thermo-, and electromigration coincide [41].

The magnitude of this activation energy corresponds to the measured activation energies to migration of Pt in the literature [13, 34]. We should note that the logarithm of the speed of change of resistance caused by the platinum migration (characterized by E_{a2}) below 10 eV^{-1} and approaches the resistance change resulted by the TiO_2 grain growth. From the value of 9.5 eV^{-1} migration phenomena dominate the process. These inverse energies give the temperatures of 1100 K and 1200 K, respectively. It signals that in the *lifetime curve* somewhere within this temperature range a *breakpoint* should appear as it does indeed (see in Fig. 2.6a).

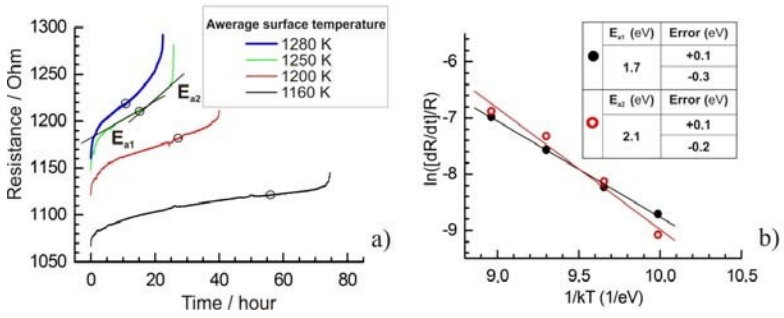

Fig. 2.5. (a) Typical resistance-time curves of double spiral Pt filaments. Each of the black circles marks the inflection-point at the curves. Black tangents indicate the slope of the curve in the vicinity of those points. (b) Arrhenius plots for the mechanisms dominating left (full dots) and right (open circles) from the inflection-point on the resistance vs. time plots. The uncertainty of the obtained activation energy values (E_{a2} and E_{a1}) is attributed to the errors in the temperature measurement [42].

Using the activation energies we could separate two main failure phenomena on the temperature scale. Consequently, the degradation of a microfilament can't be characterized by single activation energy, if more than one breakdown mechanisms of different magnitudes are present. When the temperature range above 600 °C is targeted in case of TiO_2-Pt-TiO_2 filaments, the main restrictive factor for the expected lifetime is the occurrence of phase changes in the TiO_2 adhesion layer. Nevertheless, the final killing mechanism will be the thermo- and finally the electromigration processes [42] as claimed by most literature references. In order to extend the lifetime of the Pt filament, the phase changes in the adhesion layer have to be inhibited. By selecting an appropriate adhesion layer, in which neither phase changes nor grain growth can take place at the targeted temperature, this problem can be eliminated.

Consequently in order to extend the lifetime at high temperatures, improved filament geometry and better control of degradation processes are needed. Moreover, moderate mass transport and consequently superior durability in single crystalline material are expected over the thin-film multi-crystalline metals or silicon. In the following sections novel designs of Pt filaments are investigated.

2.3.3. Temperature Distribution and Failures on the Improved Pt Filament

As indicated in Section 2.2.2. Fig. 2.3 alternative filament geometries were fabricated to improve temperature uniformity, and increase the uniformly hot heated area of the hotplate. If the catalyst is Pt the required operation temperature of the targeted methane sensitive pellistor is over 700 °C. In our previous work we demonstrated that in order to get appropriate signal - i.e. activate the catalyst on a large surface – the spiral-like meander must be heated such as the temperature in the centre is far over the required value [28]. This leads to extreme fast degradation, thereby a large plateau of the minimum required temperature must be formed. To achieve this, the filament's centre was enlarged to reduce its resistance and central heating, but keeping the temperature high by thermal conduction.

Another way is to form a ring of higher heat dissipation around the central area. In the test structures this was provided by a simple narrower ring (No.1 in Fig. 2.6) or a narrower ring with extended length (No. 2 and No. 3 in Fig. 2.6).

Furthermore, in order to reduce the inherently forming temperature gradient between the hotplate and the bulk Si, step by step widening of the contact Pt wire were formed (No. 2 and No. 3, Fig. 2.6), while extending their length.

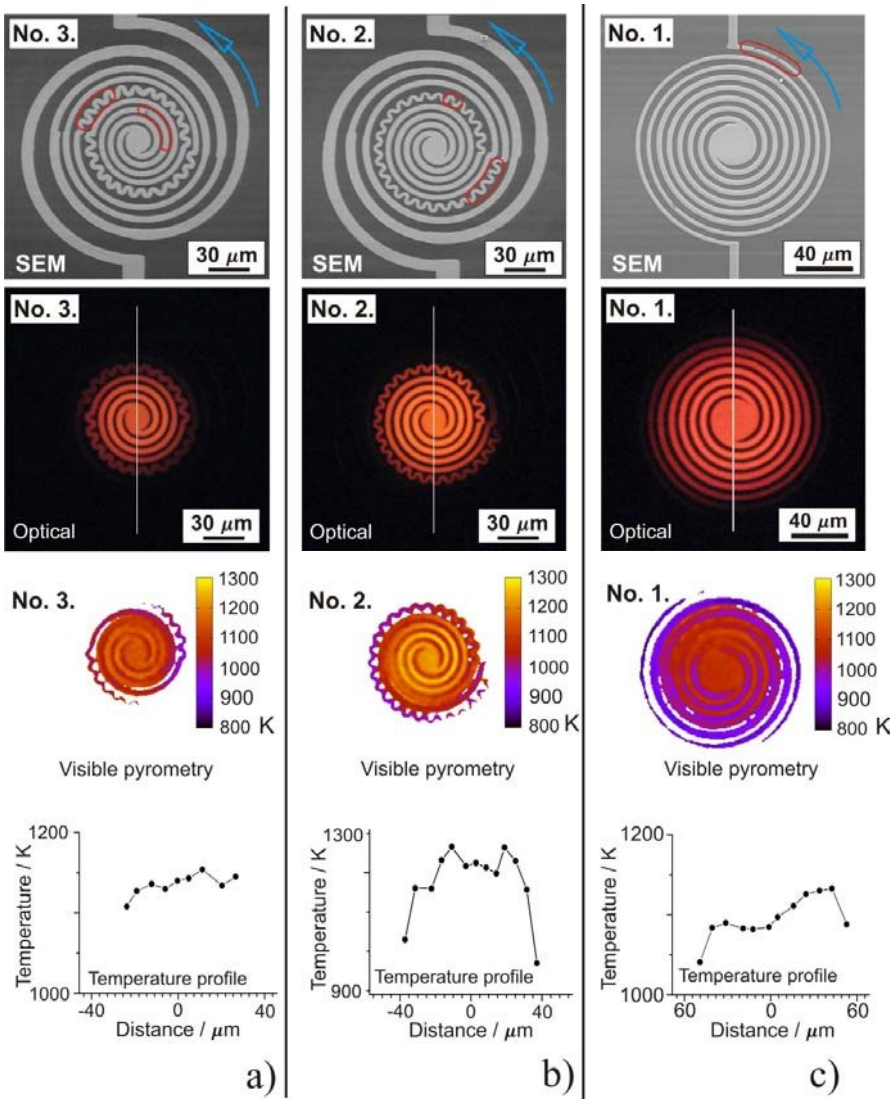

Fig. 2.6. The figure shows the SEM images, the optical images of the glowing hotplates, the corresponding temperature distribution of the heated area in the detection range of visible pyrometry, as well as the deduced temperature profile across the heater for the devices No. 1. No.2. and No. 3 in (a), (b) and (c), respectively. In the SEM images filament segments wherein the defects were identified are encircled by red line. Blue arrows indicate the direction of the electron flow.

4-4 samples of each design were tested for lifetime, whereas their temperature distribution was revealed by visible pyrometry [42].

Temperature distributions achieved show that the relatively uniform surface is enlarged to radii of c.a. 25, 30 and 50 μm for structures No. 2, No. 3 and No. 1, respectively. In No. 1 and No. 3 the difference is below 50 °C on this plateau. Compared to the earlier results given by the simple double spiral around 250-300 °C temperature drop is found at a radius of 30 μm as demonstrated in [42] or Fig. 2.8d in this chapter.

Although one of the main goals, i.e. the enlarged surface of homogeneous temperature was achieved, the temperature gradient driven deterioration couldn't be avoided yet.

In every four cases of device No.1 defect sites were observed at the same arm of the spiral along the thinnest section of the Pt filament close to the interconnections (Fig. 2.6c, SEM). However, the temperature at this section of the heated area is out of the range of visible pyrometry (below 800 K), the mass transport effects with moderated rate result faster breakdown due to the small cross section of the Pt filament. In design No. 2 and No. 3 most of the defects were formed close to end of the wavy part of the filament in all cases at given current direction (Fig. 2.6a, b, SEM). This may be the consequence of fast temperature drop along that part of the filament when the wire exits the uniform temperature region. The thicker Pt wire represents better heat condutction, thereby increases the thermal gradients at this section as it is seen in the optical and visible pyrometry images (Fig. 2.6a, b).

2.3.4. Summary of Lifetime Measurements

Lifetime of Pt filament microheaters of the above filament geometries cantilever hotplate as a reference, as well as of a full-membrane meander type heater was tested between 800-1200 K. Additionally, a single-crystal silicon filament was also tested using the same conditions (Fig. 2.7a).

In case of the double meander cantilever type microheater in Fig. 2.7 the lifetime characteristics prooved the correlation with activation energies of the failure mechanisms as described in Section 2.3.2. The position of the breakpoint appeared namely between 1100-1200 K. Meander type filament showed the shortest lifetime. This is due to the cumulative impact of encountered high thermal gradients and high temperature.

The lifetime of devices, where the temperature inhomogeneity is higher prevailing across the whole heated surface (Fig. 2.7e and No. 2**)** was longer than that of No.1 and No.3. This may be the consequence of higher thermal gradients at the perimeter of the central uniform part of the heated area. Although longer interconnects were applied, the temperature gradient is still to be reduced. This can be achieved by extending and gradual widening (increasing the cross secstion) of the Pt wires between the hot centre and the room temperature contact pads on the bulk. Further reduction in operation temperture obviously increases the device's lifetime.

Silicon single crystal is a promising filament material. However, the cross section of the filament (8 μm^2) exceeds that of Pt, the expected better activation energy of degradation makes it superior to poly-crystalline Si [13].

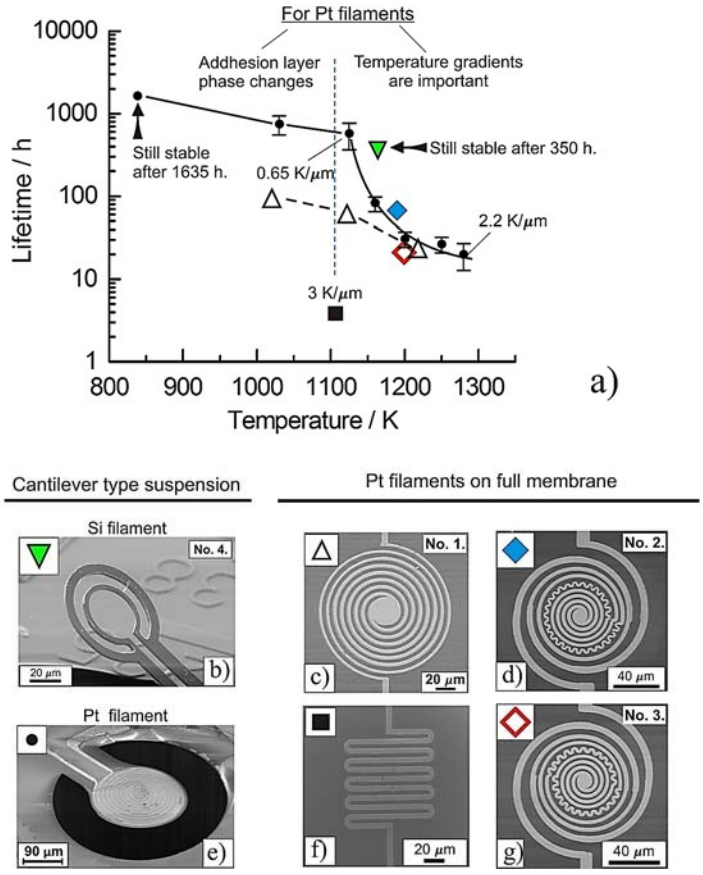

Fig. 2.7. (a) Summary of the results of lifetime measurements performed on micro-heaters with different Pt layouts and suspension designs vs. the average surface temperature. The corresponding average temperature gradients are represented for each design (b-g.). SEM images of the filaments. Filament (e) and (f) had been published earlier and the properties of the filaments detailed in [41] by the authors.

Finally, we may conclude that double spiral cantilever type Pt heaters of the investigated geometry can operate at 1000 K 1000 hours and below this temperature far longer. The lifetime of single crystal silicon heater is definitely superior to their Pt counterparts.

2.3.5. Reliability of AAO Thin Film Catalyst

Most of the microhotplates are used in gas sensors. MOX sensors utilize low-medium temperatures up to typically 300-400 °C with minimum risk of filament or hotplate degradation. From our measurements with the presented structures a lifetime of minimum

a few tens of thousands hours is obtained. When thermocatalytic gas sensors are considered, one must calculate with much higher temperature and the related degradation issues. Degradation, however, is not limited to the filament but also the reliability of the deposited catalyst must be taken into account. Catalysts can be deposited on the hotplate in various forms [43]. One of the most promising methods is the porous catalyst thin film Pd and/or Pt dispersed in Anodic Aluminium oxide (AAO) [7, 28].

To analyze the deterioration of an AAO-Pt catalyst layer, the top surface of a cantilever type micro-heater was coated by 700 nm thick porous AAO and the pore structure was covered with nanocrystals of Atomic Layer Deposition (ALD) deposited Pt. [28, 57]. These sensors were driven by constant power (42.5 mW) for 20 hours. SEM images were taken from the surface of the catalyst layer after 1 hour of operation (Fig. 2.8 b, c).

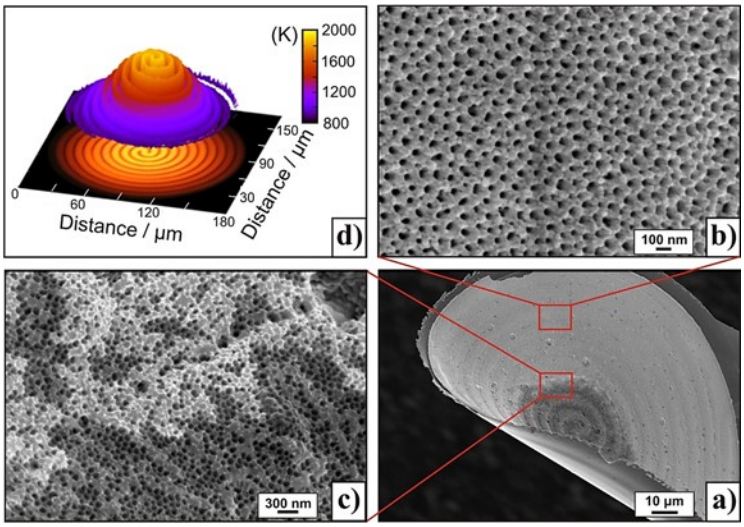

Fig. 2.8. (a) View of the AAO-Pt catalyst layer after 1 hour of operation by heating of 42.5 mW. Pt catalyst has already disappeared in the middle of the microheater and the membrane is seriously bended. (b) At the perimeter of the heated area the Pt coating is still intact. (c) Lateral migration of Pt catalyst at the surface of porous AAO support layer is evident. (d) Inhomogeneous temperature distribution was identified by visible pyrometry [41].

In Figs. 2.8c and 2.8d one can observe that platinum disappeared from the centre of the heater and started to migrate towards the perimeter of the hotplate. This lateral migration is driven by the inhomogeneous temperature distribution and the high temperature gradient present, as revealed by visible pyrometry. After 16 hours of continuous operation all the Pt was found at the cold perimeter of the hotplate and thereby the device completely lost its functionality. In addition to Pt migration the effect of the emerging high thermo-mechanical stress in the AAO layer was detected by the rolling up of the cantilever-type membrane structure. Note, that AAO formed at room temperature is amorphous and re-crystallizes during high temperature operation. The upward bending (convex) in case of all the investigated samples is due to accumulated mechanical tensile stress, whilst the as prepared cantilevers were flat.

Electron Beam Diffraction (EBD) was performed on a piece of microhotplate, cut out from its centre by FIB preparation (Fig. 2.10a). EBD patterns proved that the amorphous AAO layer transformed to α-Al_2O_3 phase after a dehydroxylation process at 1000 K (Fig. 2.10b), [45, 44]. Ko investigated the mechanical stress in heat treated AAO films and reported a tensile stress of 2-14 GPa after heat treatment, depending on the porosity of the film [46]. Porosity of our AAO film calculated with the equation by Masuda is 0.7 [47]. Following the experimental curve given by Ko the estimated stress in our film can reach a few hundred MPa. Note that, total thickness of our membrane (without AAO) is approximately 700 nm, so the estimated stress in the porous layer is high enough to cause such an enormous distortion. Consequently, the multilayer membrane structure must be tailored such, as to consider the phase transition of the AAO layer as well.

Furthermore, if the thermo-migration of Pt catalyst is present, and it plays detrimental role, one has to consider not only the lateral effect but the migration in perpendicular direction as well. Thereby, migration may take place inside the pores directed definitely from the hot filament towards the colder surface. This phenomenon is the consequence of the normal temperature gradient, induced by the heat dissipation of the micro-heater.

XTEM images of the as prepared AAO-Pt catalyst show the continuous Pt coating in inner surface of the pores (Fig. 2.9). XTEM images taken from a sample after 20 hours of operation at approx. 1300 K, however, reflect that Pt completely disappeared from the pores (Fig. 2.10a).

Pt particles tend to migrate due to the thermal agitation at elevated temperatures accompanied by high temperature gradients in the pores and on the surface of catalyst support. The undesirable motion of particles led to their agglomeration at the cold perimeter which is one form of device combustion-type gas sensor degradation.

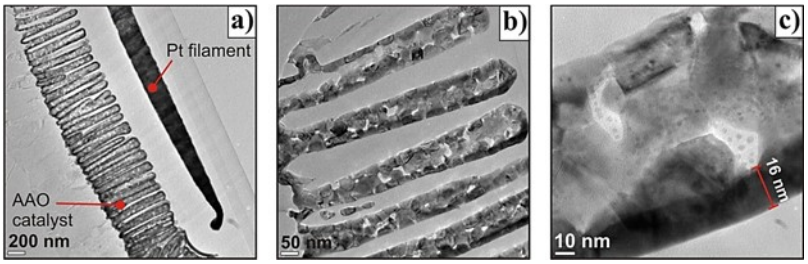

Fig. 2.9. (a) Cross section of an as-prepared microhotplate integrated with AAO-Pt catalyst formed by ALD. (b) Higher magnification shows that the pores are completely covered with Pt. (c) The schematics depicts the thickness of 16 nm Pt catalyst film in a pore.

According to literature micro-pellistors dissipate approximately 70-95 % of Joule heat to the ambient from the surfaces of the heated area [8, 29, 30]. In our case this value is 95 % i.e. to estimate the magnitude of normal temperature gradient we have to consider that cantilever type micropellistors dissipate this part of the heating power by conduction to the ambient through the top and bottom surfaces of the heated area [41]. The total thermal resistance of the porous AAO layer (top) using the thermal conductivity of

AAO [58] and the SiO_2-Si_3N_4 multilayer [37] (bottom) amounts to 74 K/W and 0.3 K/W, respectively. Because of the net thermal resistance of the microheater (30000 K/W) exceeds the thermal conductivity of the layers, we assume that approximately half of the input power is dissipated by each surface.

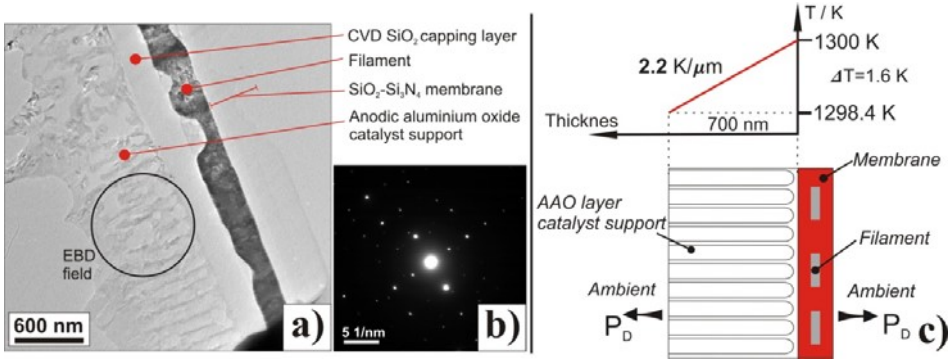

Fig. 2.10. (a) XTEM image of the sample prepared from the mid of a micropellistor operated at 42.5 mW for 20 h. (b) Electron diffraction pattern of the AAO sample. According to the EBD pattern of the re-crystalized AAO support layer is crystalline α-Al_2O_3. (c) Temperature distribution through the AAO layer for the estimation of temperature gradient normal to the AAO layer surface.

Driving the device by 42.5 mW means a temperature at the center of the hotplate of 1300 K [41]. In this sense, the temperature drop and thermal gradient across the AAO layer amount to 1.6 K and 2.2 K/μm, respectively (Fig. 2.10c).

Temperature gradients of similar magnitudes were found in the filaments also, but the migration proceeds faster in the AAO support layer. This may be the consequence of the poor adhesion between Pt grains and AAO support. Furthermore, the phase transformation mechanism of the AAO layer may also decrease the adhesion [44, 45]. These phase changes were concluded from the EBD patterns proving that the as-prepared amorphous porous AAO layer transformed to α-Al_2O_3 during the test (Fig. 2.10b).

2.4. Summary and Conclusions

The lifetime of microhotplates becomes crucial with required operation temperature in excess of 500 - 550 °C. As the most common application at this temperature is the thermocatalytic detection of methane, we investigated the deterioration mechanisms of Pt filament and Pt catalyst activated micropellistror structures.

Tree basic phenomena were identified in course of the continuing deterioration leading to the final rupture of the filament. Next to the previously reported phase transitions and electro-migration effects the crucial role of the temperature gradient induced thermo-migration along the filament was revealed. The non-uniform temperature distribution also generates the migration of the Pt catalyst towards the coldest area and finally leads to the complete loss of catalytic activity.

From these results we conclude that the hotplate of a high temperature operated micro-pellistor must have the following features (apart of the known thermomechanical constraints):

- Large surface with uniform temperature;
- Temperature gradients of less than 0.5 K/μm in the area, where the temperature is >500 °C; (This is definitely true for multi-crystalline Pt and other metal filaments. The corresponding value for a crystalline Si meander is still to be investigated);
- A temperature barrier around the catalyst coated area, i.e. a higher temperature ring framing the uniform temperature active area to prevent catalyst migration towards the perimeter.

In summary the selection of filament material and layout of the filament/hotplate play essential role in stability. Nevertheless, we have to emphasize that the most straightforward way to prolongation of lifetime is to find appropriate catalyst effective even at reduced temperatures.

Acknowledgements

This work was partially supported by the Hunarian Russian bilateral project No. 2017-2.3.4-TÉT-RU-2017-00006.

The useful discussions with Alexey Vasiliev and Nikolay Samotaev are gratefully acknowledged.

References

[1]. S. Kulinyi, D. Brandszájsz, H. Amine, M. Ádám, P. Fürjes, I. Bársony, Cs. Dücső, Olfactory detection of methane, propane, butane and hexane using conventional transmitter norms, *Sensors and Actuators B*, Vol. 111-112, 2005, pp. 286-292.

[2]. F. Völklein, M. Grau, A. Meier, L. Breuer, P. Woias, Optimized MEMS Pirani sensor with increased pressure measurement sensitivity in the fine and high vacuum regime, *Journal of Vacuum Science and Technology A: Vacuum, Surfaces and Films*, Vol. 31, Issue 6, 061604.

[3]. P. Fürjes, G. Légrádi, Cs. Dücső, I. Bársony, Thermal characterisation of a direction dependent flow sensor, *Sensors and Actuators A*, Vol. 115, Issue 2, 2004, pp. 417-423.

[4]. P. A. Bartlett, S. Guerin, A micro machined calorimetric gas sensor: An application of elecrtodeposited nanostructured palladium for the detection of combustible gases, *Analytical Chemistry*, Vol. 75, 2003, pp. 126-132.

[5]. P. Fürjes, Zs. Vízváry, M. Ádám, I. Bársony, A. Morrissey, Cs. Dücső, Materials and processing for realization of microhotplates operated at elevated temperature, *Journal of Micromechanics and Microengineering,* Vol. 12, 2002, pp. 425-429.

[6]. J. Courbat, D. Briand, N. F. de Rooji, Reliability improvement of suspended platinum based micro-heating elements, *Sensors and Actuators A*, Vol. 142, 2008, pp. 284-291.

[7]. Q. Chen, H. Dong, S. Xia, A novel micro-pellistor based on nanoporous alumina beam support, *Journal of Electronics (China)*, Vol. 29, Issue 5, 2012, pp. 469-472.

[8]. A. Pike, J. W. Gardner, Thermal modelling and characterisation of micropower chemoresistive silicon sensors, *Sensors and Actuators B*, Vol. 45, 1997, pp. 19-26.
[9]. M. Gall, The Si planar pellistor: A low power pellistor sensor is Si thin film technology, *Sensors and Actuators B*, Vol. 4, 1991, pp. 533-538.
[10]. L. Xu, T. Li, X. Gao, Y. Wang, Design and fabrication of a novel 3D micropellistor, in *Proceedings of the 14th International Meeting on Chemical Sensors (IMCS'12)*, Nuremberg, Germany, 20-23 May 2012, pp. 440-443.
[11]. H. Gao, J. Amann, X. Lyu, J. Wöllenstein, S. Palzer, Novel method for thermal characterisation of MEMS, *Journal of Microelectromechanical Systems*, Vol. 27, Issue 3, 2018, pp. 521-528.
[12]. E. E. Karpov, E. F. Karpov, A. Suchkov, S. Mironov, A. Baranov, V. Sleptsov, L. Calliari, Energy efficient planar catalytic sensor for methane measurement, *Sensors and Actuators B*, Vol. 194, 2013, pp. 176-180.
[13]. J. Spannhake, O. Schulz, A. Helwig, A. Krenow, G. Müller, T. Doll, High-temperature heater platforms: Long performance of metal and semiconductor heater materials, *Sensors*, Vol. 6, 2006, pp. 405-419.
[14]. M. Graf, D. Barrettino, K. Kirstein, A. Hierlemann, CMOS microhotplate sensor system for operating temperatures up to 500 °C, *Sensors and Actuators B Chemical*, Vol. 117, Issue 2, 2006, pp. 346-352.
[15]. Cs. Dücső, É. Vázsonyi, M. Ádám, I. Bársony, J. G. E. Gardeniers, A Van Den Berg, Porous silicon bulk micromachining for thermally isolated membrane formation, *Sensors and Actuators A*, Vol. 60, 1997, pp. 235-239.
[16]. C. Tsamis, A. G. Nassiopoulou, A. Tserepi, Thermal properties of suspended porous silicon microhotplates for sensor applications, *Sensors and Actuators B,* Vol. 95, 2003, pp. 78-82.
[17]. J. Lee, W. P. King, Microcantilever hotplates: Design, fabrication and characterisation, *Sensors and Actuators A*, Vol. 136, 2007, pp. 291-298.
[18]. R. P. Manginell, J. H. Smith, A. J. Ricco, D. J. Moreno, R. C. Hughes, Selective Pulsed CVD of Platinum on Microfilament Gas Sensors*, Office of Scientific and Technical Information Technical Reports*, 1996.
[19]. H. Ma, S. Qin, L. Wang, G. Wang, X. Zhao, E. Ding, The study of methane sensing with high temperature low-power CMOS compatible silicon microheater, *Sensors and Actuators B*, Vol. 244, 2017, pp. 17-23.
[20]. G. F. Fine, L. M. Cavanagh, A. Afonja, R. Binions, Metal oxide semi-conductor gas sensors in environmental monitoring (Review), *Sensors*, Vol. 10, Issue 6, 2010, pp. 5469-5502.
[21]. L. M. Phinney, M. S. Baker, J. R. Serrano, Microelectromechanical Systems and Devices, Dr. Nazmul Islam, *InTech*, 2012.
[22]. P. Dubois, E. Vela, S. Koster, D. Briand, H. R. Shea, N. F. de Rooji, Paraffin-PDMS composite thermo microactuator with large vertical displacement capability, *Actuator,* Bremen, 2006, pp. 215-218.
[23]. S. Ogden, L. Klintberg, G. Thornell, R. Bodén, Review on miniaturized paraffin phase change actuators, valves and pumps, *Microfluidics and Nanofluidics*, Vol. 17, Issue 1, 2013, pp. 57-71.
[24]. H. Ishihara, K. Masunao, M. Ishii, S. Kumagai, M. Sasaki, Enhanced Plasmonic Wavelength Selective Infrared Emission Combined with Microheater, *Materials*, Vol. 10, 2017, pp. 1085-1093.
[25]. W. Streyer, K. Feng, Y. Zhong, A. J. Hoffman, D. Wasserman, Selective absorbers and for far-infrared wavelengths, *Applied Physics Letters,* Vol. 107, Issue 8, 2015, 081105.
[26]. J. F. Creemer, S. Helveg, G. H. Hoveling, S. Ullmann, P. J. Kooyman, A. M. Molenbroek, H. W. Zandbergen, P. M. Sarro, MEMS nanoreactor for atomic-resolution microscopy of nanomaterials in their working state, in *Proceedings of the IEEE 22nd International*

Conference on Micro Electro Mechanical Systems (MEMS'09), Sorrento, Italy, 25-29 January, 2009, pp. 76-79.
[27]. T. Guan, R. Puers, Thermal Analysis of a Ag/Ti Based Microheater, *Procedia Engineering*, Vol. 5, 2010, pp. 1356-1359.
[28]. F. Bíró, Cs. Dücső, Gy. Z. Radnóczi, Zs. Baji, M. Takács, I. Bársony, ALD nano-catalyst for micro-calorimetric detection of hydrocarbons, *Sensors and Actuators B Chemical*, Vol. 247, 2017, pp. 617-625.
[29]. M. Zanini, J. H. Visser, L. Rimai, R.E. Soltis, A. Kovalchuk, D. W. Hoffman, E. M. Logothetis, U. Bonne, L. Brewer, O. W. Bynum, M. A. Richard, Fabrication and properties of a silicon based high-sensitivity microcalorimetric gas sensor, *Sensors and Actuators A,* Vol. 48, 1995, pp. 187-192.
[30]. R. Triantafyllopoulou, S. Chatzandroulis, C. Tsamis, A. Tserepi, Alternative microhotplate design for low power sensor arrays, *Microelectronics Engineering*, Vol. 83, 2006, pp. 1189-1191.
[31]. A. Harley-Trochimczyk, A. Rao, H. Long, A. Zettl, C. Carraro, R. Maboudian, Low-power catalytic gas sensing using highly stable silicon carbide microheaters, *Journal of Micromechanics and Microengineering*, Vol. 27, 2017, pp. 045003-045013.
[32]. W. J. Hwang, K. S. Shin, J. H. Roh, D. S. Lee, S. H. Choa, Development of microheaters with optimized temperature compensation design for gas sensors, *Sensors*, Vol. 11, 2011, pp. 2580-2591.
[33]. D. Briand, G. M. Tomassone, N. F. de Rooji, Accelerated ageing of micro-hotplates for gas sensing applications, in *Proceedings of the IEEE Conference on Sensors (SENSORS'03),* Toronto, Canada, 2003, pp. 1314-1317.
[34]. R. Rusanov, H. Rank, J. Graf, T. Fuchs, R. Mueller-Fiedler, O. Kraft, Reliability of Pt electrodes and heating elements on SiO_2 insulation layers and membranes, *Microelectronics Reliability*, Vol. 55, 2015, pp. 1920-1925.
[35]. D. Resnik, U. Aljancic, D. Vrtacnik, M. Mozek, S. Amon, Mechanical stress in thin film microstructures on silicon substrate, *Vacuum*, Vol. 80, 2005, pp. 236-240.
[36]. C. Rossi, P. Temple-Boyer, D. Esteve, Realization and performance of thin SiO_2/SiN_x membrane for micro-heater applications, *Sensors and Actuators A*, Vol. 64, 1998, pp. 241-245.
[37]. J. Laconte, D. Flandre, J. P. Raskin, Micromachined Thin Film Sensors for SOI-CMOS Co-integration, *Springer*, 2006, pp. 47-103.
[38]. U. Dibbern, A substrate for thin-film gas sensors in microelectronic technology, *Sensors and Actuators B*, Vol. 2, 1990, pp. 63-70.
[39]. K. D. Hurley, B. G. Frederick, W. J. DeSisto, A. R. P. van Heiningen, M. Clayton Wheeler, Catalytic reaction characterization using micromachined nanocalorimeters*, Applied Catalysis A: General*, Vol. 390, 2010, pp. 84-93.
[40]. D. Spirjakin, A. M. Baranov, A. Somov, V. Sleptsov, Investigation of heating profiles and optimization of power consumption of gas sensors for wireless sensor network*, Sensors and Actuators A: Physical*, Vol. 247, 2016, pp. 247-253.
[41]. F. Bíró, Z. Hajnal, Cs. Dücső, I. Bársony, The critical impact of temperature gradients on Pt filament failure, *Microelectronics Reliability*, Vol. 78, 2017, pp. 118-125.
[42]. F. Bíró, Z. Hajnal, C. Dücső, I. Bársony, The role of phase changes in $TiO_2/Pt/TiO_2$ filaments, *Journal of Electronic Materials*, Vol. 47, Issue 4, 2018, pp. 2322-2329.
[43]. E. Vereshchagina, O. Blyzniuk, R. M. Tiggelaar, K. Altena-Schildkamp, J. G. E. Gardeniers*,* Local deposition and patterning of catalytic thin films in microsystems, *Journal of Micromechanics and Microengineering*, Vol. 22, 2012, pp. 045023-045034.
[44]. P. P. Mardilovich, A.G. Govyadinov, N. I. Mukhurov, A.M. Rzhevskii, R. Paterson, New and modified alumina membranes Part I. Thermotreatment of anodic alumina membranes, *Journal of Membrane Science*, Vol. 98, Issue 1-2, 1995, pp. 143-155.

[45]. M. Kylan McQuaing Jr., A. Toro, W. Van Geertruiden, W. Z. Misiolek, The effect of high temperature heat treatment on the structure of anodic aluminium-oxide, *Journal of Material Science*, Vol. 46, 2011, pp. 243-253.
[46]. S. Ko, D. Lee, S. Jee, H. Park, K. Lee, W. Hwang, Mechanical properties and residual stress in porous anodic alumina structures, *Thin Solid Films*, Vol. 515, 2006, pp. 1932-1937.
[47]. H. Masuda, K. Fukuda, Ordered metal nanohole arrays made by a two-step replication of honeycomb structures of anodic alumina, *Science*, Vol. 9, Issue 268, 1995, pp. 1466-1474.
[48]. F. Udrea, J. W. Gardner, D. Setiadi, J. A. Covington, T. Dogaru, C. C. Lu, W. I. Milne, Design and simulation of SOI CMOS micro-hotplate gas sensor, *Sensors and Actuators B,* Vol. 78, 2001, pp. 180-190.
[49]. L. Xu, T. Li, X. Gao, Y. Wang, Development of a reliable micro-hotplate with low power consumption, *IEEE Sensors Journal*, Vol. 11, Issue 4, 2011, pp. 913-919.
[50]. I. Bársony, P. Fürjes, M. Ádám, Cs. Dücső, Zs. Vízváry, J. Zettner, F. Stam, Thermal response of microfilament heaters in gas sensing, *Sensors Actuators B*, Vol. 103, 2004, pp. 442-447.
[51]. J. C. Belmonte, J. Puigcorbe, J. Abriol, A. Vila, J. R. Morante, N. Sabate, I. Garcia, C. Cane, High-temperature low-power performing micromachined suspended microhotplate for gas sensing applications, *Sensors Actuators B*, Vol. 114, 2006, pp. 826-835.
[52]. J. F. Creemer, D. Briand, H. W. Zandbergen, V. van der Vlist, C. R. de Boer, N. F. de Rooij, P. M. Sarro, Microhotplates with TiN heaters, *Sensors and Actuators A*, Vol. 148, 2008, pp. 416-421.
[53]. J. Puigcorbé, D. Vogel, B. Michel, A. Vilà, I. Gràcia, C. Cané, J. R. Morante, High temperature degradation of Pt/Ti electrodes in micro-hotplate gas sensors, *Journal of Micromechanics and Microengineering*, Vol. 13, 2003, S119.
[54]. J. Puigcorbé, D. Vogel, B. Michel, A. Vilà, I. Gràcia, C. Cané, J. R. Morante, Thermal and mechanical analysis of micromachined gas sensors*, Journal of Micromechanics and Microengineering*, Vol. 13, 2003, pp. 548-556.
[55]. E. M. F. Vieira, J. F. Ribeiro, R. Sousa, M. M. Silva, L. Dupont, L. M. Goncalves, Titanium oxide adhesion layer for high temperature annealed $Si/Si_3N_4/TiO_x/Pt/LiCoO_2$ battery structures, *Journal of Electronics Materials*, Vol. 45, Issue 2, 2016, pp. 910-916.
[56]. J. M. Bosc, Guo, V. Sarihan, T. Lee, Accelerated life testing for micro-machined chemical sensors, *IEEE Transactions on Reliability*, Vol. 47, Issue 2, 1998, pp. 135-141.
[57]. F. Bíró, G. Z. Radnóczi, M. Takács, Z. Baji, C. Dücső, I. Bársony, Pt deposition techniques for catalytic activation of nano-structured materials*, Procedia Engineering*, Vol. 168, 2016, pp. 1148-1151.
[58]. A. Begona, J. Maiz, M. M. Gonzalez, Rules to determine thermal conductivity and density of Anodic Aluminum Oxide membranes, *The Journal of Physical Chemistry*, Vol. 120, 2016, pp. 5361-5370.